Colloquia: IFA 2010

Channeler Ant Model: 3D segmentation of medical images through ant colonies

E. Fiorina(1)(2), R. Arteche Diaz(3)(2), P. Bosco(4)(5), G. Gargano(6)(7),
A. Massafra(8)(9), R. Megna(6)(7), C. Oppedisano(2) and S. Valzano(1)(2)

(1) Dipartimento di Fisica Sperimentale, Università di Torino - Torino, Italy
(2) INFN, Sezione di Torino - Torino, Italy
(3) CEADEN - Havana, Cuba
(4) Dipartimento di Fisica, Università di Genova - Genova, Italy
(5) INFN, Sezione di Genova - Genova, Italy
(6) Dipartimento Interateneo di Fisica, Università di Bari - Bari, Italy
(7) INFN, Sezione di Bari - Bari, Italy
(8) Dipartimento di Fisica, Università del Salento - Lecce, Italy
(9) INFN, Sezione di Lecce - Lecce, Italy

Summary. — In this paper the Channeler Ant Model (CAM) and some results of its applications to the analysis of medical images are described. The CAM is an algorithm able to segment 3D structures with different shapes, intensity and background. It makes use of virtual ant colonies and exploits their natural capabilities to modify the environment and communicate with each other by pheromone deposition. Its performance has been validated with the segmentation of 3D artificial objects and it has been already used successfully in lung nodules detection on Computer Tomography images. This work tries to evaluate the CAM as a candidate to solve the quantitative segmentation problem in Magnetic Resonance brain images: to evaluate the percentage of white matter, gray matter and cerebrospinal fluid in each voxel.

PACS 07.05.Mh – Neural networks, fuzzy logic, artificial intelligence.
PACS 87.57.R- – Computer-aided diagnosis.
PACS 87.57.-s – Medical imaging.
PACS 87.57.Q- – Computed tomography.

1. – Introduction

The Channeler Ant Model (CAM) [1] is developed by the MAGIC5 Collaboration with the purpose of implementing a Computer Aided Detection (CAD) system for the lung cancer diagnosis. The CAM makes use of virtual ant colonies to segment 3D complex structures.

1`1. *Swarm Intelligence*. – Swarm Intelligence is the feature of a system whose collective behaviour produces the rising of patterns characteristic of the system. In it each agent has limited knowledge and capabilities and does not know the global state of the system. The agents interact by modifying the environment through the deposition of pheromones.

These systems are characterized by stigmergy, non-linearity and chaos, emergence and self-organization. Social insects like ants belong to a super-organism composed by many agents: the perception of the colony is the sum of perceptions of all its members and if an ant is not smart, the colony is.

Forging, cemetery building, larvae feeding and brood sorting are characterized by intelligence. In all these activities the communication between agents plays an important role.

Studies on real ants life show that pheromone power is not linear and it is a function of:

  – the sensory capability, that reaches a saturation point beyond which the perception of pheromone does not change with the quantity released;

  – the ant's osmotropotaxis sensitivity, that is an intrinsic parameter of the way ants use to smell pheromone and is linked to the degree of randomness according to which the ants follow the pheromone trails.

In nature the pheromone power also depends on the ant's speed, on ant's antennas size and on the angle under which ants smell the trails. Furthermore, the pheromone trails evaporate and diffuse: that makes the colony able to choose the shortest way, *e.g.*, from the nest to food resource.

1`2. *Virtual ant colonies*. – Virtual ant colonies were used to solve many optimization and segmentation problems.

In 1995 Chialvo and Millonas [2] introduced one of the simplest and most efficient models of trail forming where the ants are moving in a 2D environment searching food. In their paper the pheromone trails created by ants are compared to the cognitive brain map patterns. Ramos and Almeida [3] developed a virtual ant model where the colonies are given by a constant number of ants that live in a digital habitat and, in particular, in an image. They proved the ants capability to reprocess different types of digital habitat reaching in the end a global perception of the image. In this model a mechanism that self-regulates the population by using the concepts of ageing, death and reproduction in the ant colony is introduced.

In 2005 Bocchi *et al.* [4] proposed an image segmentation method that makes use of an evolutionary swarm-based algorithm in which different populations of individuals compete to occupy the 2D image to be analyzed. The comparison to other techniques showed an improvement in the segmentation of noisy images.

A virtual-ant–based approach was also applied to solve other open questions like the problem of load balancing and message routing in telecommunications (Schoonderwoerd *et al.* [5]) and the Travelling Salesman Problem (TSP) (Dorigo [6]).

2. – CAM rules

The CAM rules implement the ants' movement, the ants' pheromone deposition and the ants' life. In particular, through a life parameter called energy, death and reproduction take place.

2˙1. *Movement*. – The probability to choose the voxel v_j for an ant that is in the voxel v_i is

$$(1) \qquad P_{ij}(v_i \rightarrow v_j) = \frac{W(\sigma_j)}{\sum_{n=1}^{26} W(\sigma_n)},$$

where W is a function of the pheromone quantity σ_j released in the voxel v_j:

$$(2) \qquad W(\sigma_j) = \left(1 + \frac{\sigma_j}{1 + \delta\sigma_j}\right)^{\beta},$$

β and δ are parameters determined by studies on real ants: they tell respectively how strongly pheromone trails attract ants and which is the ants sensitivity in perceiving pheromone.

In the beginning, movements are random but, later, pheromone trails become more and more important for choosing the future destination.

An ant cannot move to a voxel occupied by another ant or outside the volume of interest (called *habitat*) or in which a fixed maximum pheromone amount (*threshold*) is reached. This last constraint is implemented to simulate in a easy way the effects of pheromone evaporation. If an ant does not have possible future destination dies.

2˙2. *Pheromone deposition*. – Each ant, before moving, releases a quantity of pheromone T given by

$$(3) \qquad T = \eta + H_{fac}\Delta_{ph},$$

η and H_{fac} are constants: the first is very small and is used to mark the voxels visited from the voxels not visited, the second, together with the fixed pheromone threshold, is related to algorithm speed.

Δ_{ph} plays a crucial role in image segmentation. It represents the connection between the image intensity and the ant perception of it, it is the link between the real and the virtual world.

In the CAM validation and in its applications reported in this paper, Δ_{ph} is defined by

$$(4) \qquad \Delta_{ph} = I(v_j) - I_{min},$$

where $I(v_j)$ is the image intensity of the voxel v_j and I_{min} is the minimum intensity of the image.

If Δ_{ph} is calculated with eq. (4) the ant colonies segment voxels with a high intensity value: changing the Δ_{ph} definition it is possible to segment volumes with different intensity features.

2˙3. *Energy: Birth, reproduction and death*. – Each ant is born with an energy E_0:

$$(5) \qquad E_0 = 1 + \alpha$$

and lives in a range of energy from E_d, energy of death, to E_r, energy of reproduction. The true free parameter that manages the colony evolution is $(E_r - E_d)/\alpha$.
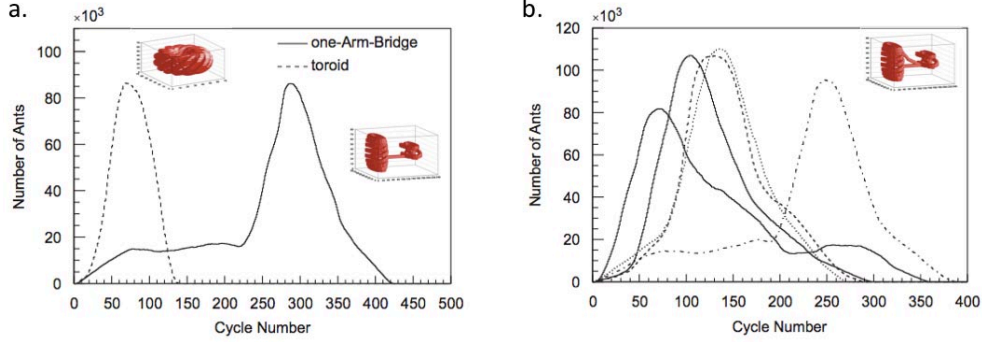
Fig. 1. – a. Colony evolution in objects with different shape; b. colony evolution in Two-Arm-Bridge object with different anthill position.

At the cycle $i + 1$ the energy of the ant k is given by

$$E_{i+1}^k = E_i^k + \alpha \left(\frac{\Delta_{ph}^k(i+1)}{\langle \Delta_{ph} \rangle_{tot}} - 1 \right),$$

(6)

where $\Delta_{ph}^k(i+1)$ is the pheromone released by the ant k in the cycle $i+1$ and $\langle \Delta_{ph} \rangle_{tot}$ is the average of all pheromone releases in the colony life.

When an ant reaches the energy of reproduction, the maximum number of ants that is possible to generate is calculated. It is a function of the image intensity: the higher is the average pheromone that could be deposited in the neighbour voxels, the more ants are generated with an upper limit set to 26 (all the voxel neighbours). Then a check over the number of free neighbour voxels is made and then the ants that is possible to generate in a free voxel born.

An ant dies if the energy is lower then E_d or if the ant has not a possible future destination.

3. – Colony evolution

The colony starts its evolution from the anthill set in a voxel that belongs to the object to be segmented. At the beginning 26 ants are generated in the way described before. Then they start moving randomly in the environment releasing pheromone. Cycle after cycle the pheromone power becomes more and more important. When in a voxel the pheromone threshold value is reached, that destination becomes forbidden. This constraint makes the ant colony a self-normalized system. When the ants explored and saturated the voxels that belong to the object to segment, they move outside it, lose energy and then die.

Colony evolution is a function of the object complexity and the anthill location.

This is shown in the results obtained on the artificial objects used for the validation [1].

In fig. 1a the colony evolution to segment two different artificial objects (a One-Arm-Bridge and a Toroid) are shown. The Toroid pattern is triangular-like while the One-Arm-Bridge one is different because the location of the anthill along the thin bridge limits the population increase until the thicker part of the object is reached.
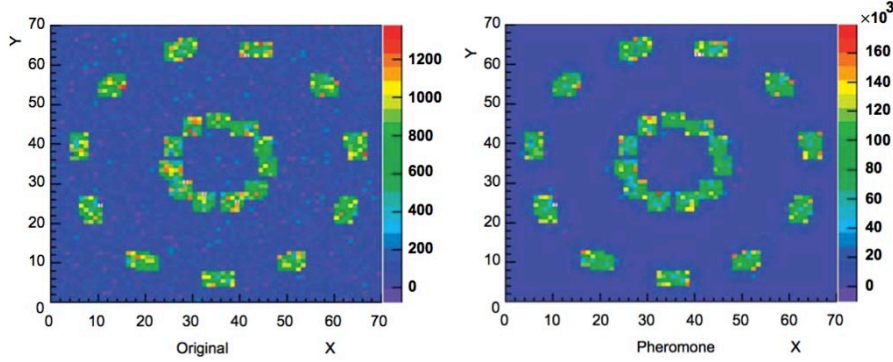
Fig. 2. – The Toroid original image and the corresponding pheromone map.

In fig. 1b the different colony evolutions from different anthill positions are shown for the Two-Arm-Bridge. The peaks correspond to the segmentation of the two arms, while the plateau is given by the bridge segmentation. Even if the evolution patterns are different, the sensitivity is compatible and this shows that the CAM performance does not depend on the anthill location.

4. – Results

4̇1. *CAM Validation on Artificial Objects* [1]. – The artificial objects have known features (shape, noise, intensity, uniformity) that could be changed and are a known gold standard which can be used to evaluate the CAM segmentation performance. They also have a smaller size than medical images ($70 \times 70 \times 70$ voxels) and so the elaboration time is shorter.

In fig. 2 the original image and the pheromone map are shown for the Toroid object. To evaluate the CAM performance some indices are defined. Sensibility S and contamination C are given by

$$(7) \qquad\qquad S = \frac{N_R}{N_T}\,,$$

$$(8) \qquad\qquad C = \frac{N_{TR} - N_R}{N_T}\,,$$

where N_R are the voxels correctly segmented, N_{TR} the total voxels segmented and N_T the voxels that must be segmented since they belong to the object.

In fig. 3a the FROC curves for all the artificial objects are reported: they prove that in objects with different shape the CAM has the same behaviour reaching the sensibility of 0.997 with a contamination equal to 0.03 for all the structures considered. In fig. 3b the FROC curves related to Highway segmentation with different noise values are shown: with increasing noise the CAM performance decreases but the sensitivity is still better than 0.95 with a contamination of 0.1.

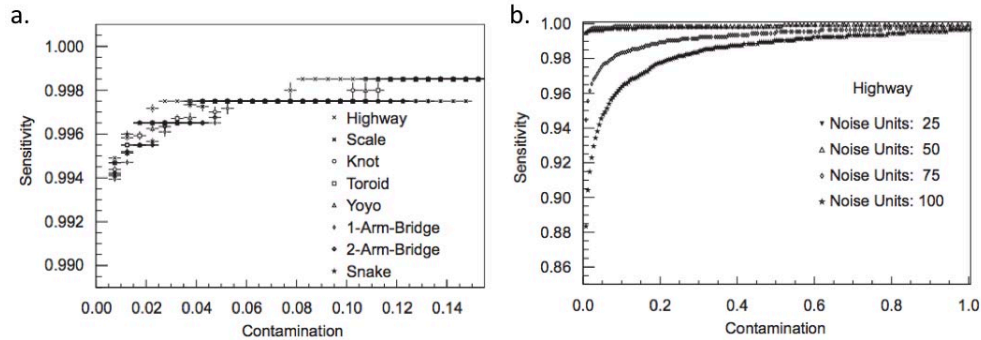4̇2. *CAM in lung CTs*. – In fig. 4 the flow diagram of the CAM lung CAD system is shown.

Fig. 3. – a. FROC curves for objects with different shape; b. FROC curves for the Highway object with different noise levels.

At the beginning the total lung volume is segmented in CTs through a region growing algorithm and this segmented mask defines the habitat in which ants live.

The CAM is then used for two different purposes. Firstly the anthill is set near the "Hilus Pulmonis" and the ant colony segments the bronchial and vascular trees, that are the most important source of false positive findings. After that, the bronchial and vascular trees are removed from the original image. In the obtained subtracted image, the CAM is used iteratively to segment the nodule candidates through an iterative procedure: until in the subtracted image there is a voxel that meets the condition to be an anthill, the ant colonies nest and evolve. The deployments built in these steps represent the nodule candidates found by CAM. Finally the list of findings is classified by a multi-layer perceptron and the result is compared to the radiologist's diagnosis.

The CAM was applied to lung CTs analysis over three samples of images from different sources (table I):

  – 5 CTs provided by ANODE09 challenge organizers and belonging to the Nelson study [7],
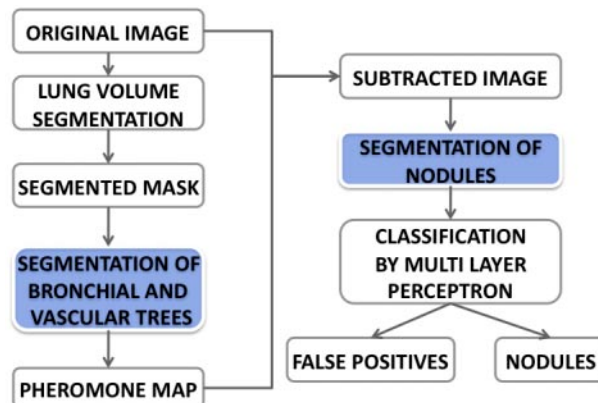

Fig. 4. – CAD structure.

TABLE I. – *Lung CTs database.*

Database	CTs scans	Slice thickness	Readers	Nodules
ANODE09	5	1 mm–0.7 mm	2 indep. + 1	39
GStest	20	< 1.25 mm	2 indep. + 1	39
LIDC	45	0.6 mm–3 mm	3	77

– 20 CTs from GStest that belongs to the ITALUNG_CT database which is the first randomized and controlled italian trial screening [8],

– 45 CTs from Lung Image Database Consortium (LIDC) site in which there are multi-center and multi-manufacturer images [9].

In fig. 5 the sensitivity as a function of the number of false findings per scan is drawn for the three samples of scans. The performance is pretty good, although likely to be improved. It is particularly interesting to remark that these CAM results were obtained without any other CAM optimization after the artificial objects validation.

4`3. *CAM in brain MRIs.* – The CAM is a good candidate also for white matter, gray-matter and cerebrospinal fluid segmentation in brain MRI images. The segmentation of brain structures is an important tool for diagnosis and progression study of brain diseases like Alzheimer's disease.

Segmenting in brain images means to determine the percentages of the different anatomical tissues present in each voxel and therefore the segmentation is a quantitative goal, not a qualitative analysis like in artificial objects or in Lung CTs.
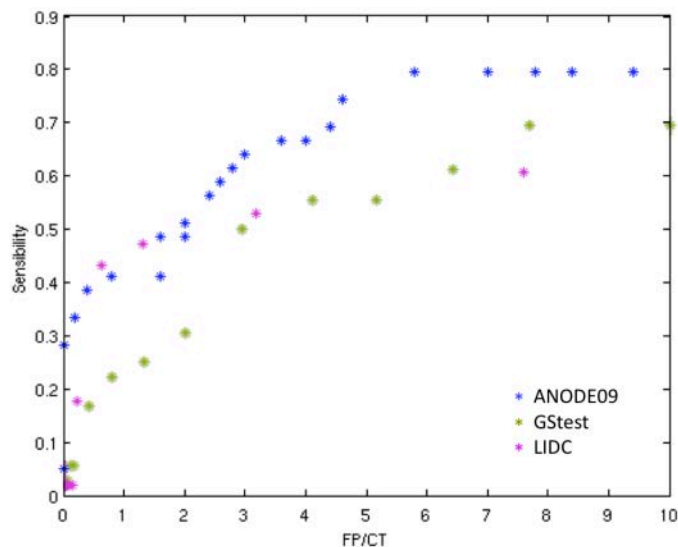

Fig. 5. – Sensitivity as a function of the number of false findings per scan for the three Lung CT databases.
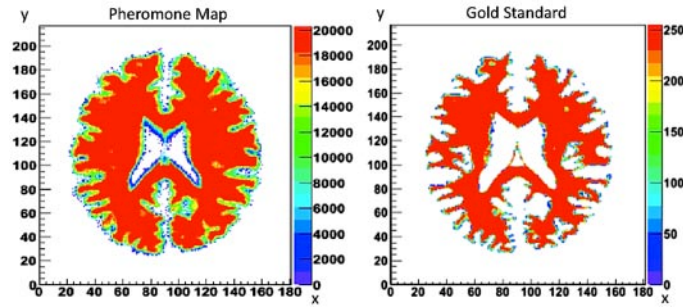
Fig. 6. – The pheromone map and the corresponding gold standard in an MRI image T1 weighted with noise 0% and RF bias field 0%.

To validate the CAM brain segmentation power the Simulated Brain Database was used. It is provided by the Brain Imaging Centre, Montreal Neurological Institute, McGill University, it is available on-line [10] and it contains a large number of brain MRI images with different noise levels (from 0% to 9%) and different RF bias-field levels (from 0% to 40%). The database also includes the images of the phantom used to obtain the simulated ones, in which, for each voxel, the intensity is proportional to the percentage of white matter. These images represent a standard segmentation and can be used as a gold standard to evaluate the CAM segmentation result.

In fig. 6 the pheromone map obtained by CAM segmentation of white matter is compared to the corresponding gold standard.

The pheromone map analysis is divided into two steps.

First the voxels that have 100% of white matter in CAM segmentation are compared to the gold standard (voxels that have 100% of white matter are represented in these 8-bit images with an intensity of 255). Figure 7 shows the ROC curve: the CAM reaches high sensitivity values (*i.e.* $S = 0.955$) with a contamination of about 0.09.
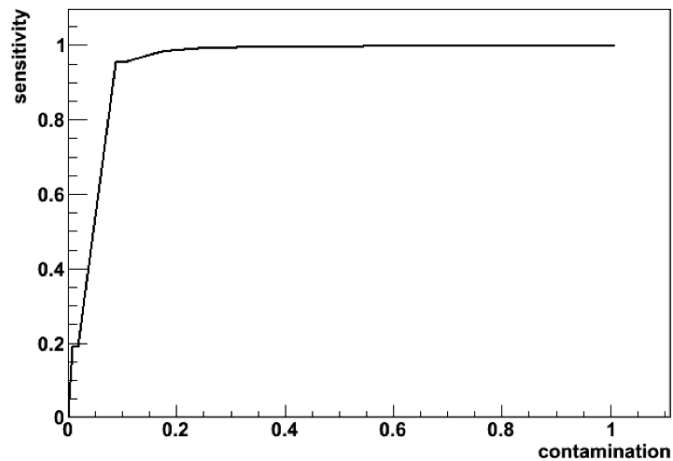

Fig. 7. – ROC curve for the voxels that reach the pheromone saturation (*i.e.* voxels segmented as 100% of white matter).
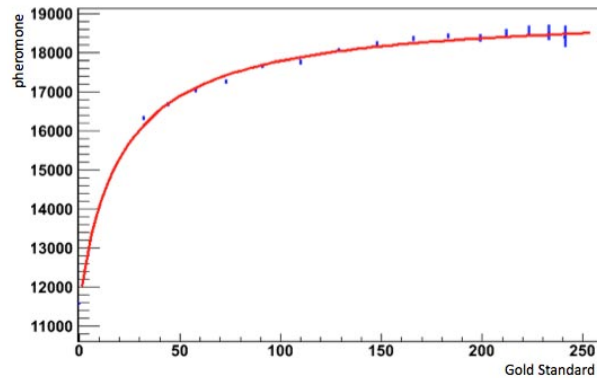
Fig. 8. – The correlation between the average pheromone deposition and the percentage of white matter.

In the second step, voxels which did not reach the pheromone saturation value are analyzed, in order to study the correlation between the pheromone deposition and the percentage of white matter, so as to be able to estimate it.

In fig. 8 the average correlation between the released pheromone and the gold standard values is shown. The red line is the result of a hyperbolic fit to the data.

Starting from the fit result and the pheromone quantity deposit in each voxel, the CAM can estimate the white matter fraction. The difference between the fraction of white matter estimated by CAM(WM) and the given gold standard (GS) normalized to the 100% of white matter, shown in fig. 9, provides the resolution and the absolute error of this method.

The vertical scale is normalized to the number of voxels that belong to the brain volume (*i.e.* voxels that contain a percentage of white matter, gray matter or cerebrospinal fluid).
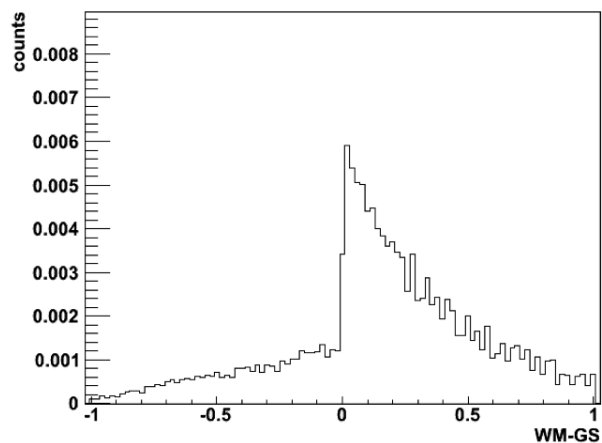

Fig. 9. – Difference between the CAM white matter estimate (WM) and the gold standard value (GS) normalized to the 100% of white matter.
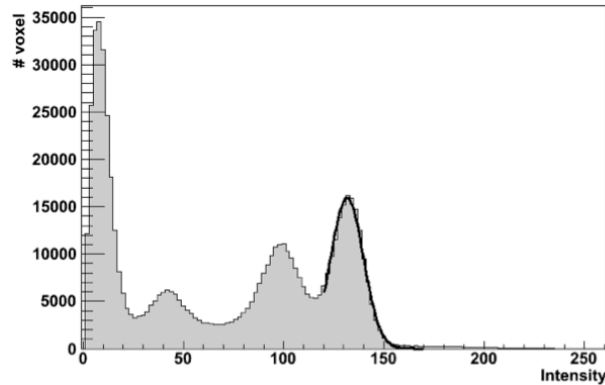
Fig. 10. – The intensity distribution of the simulated brain images with the Gaussian fit of white-matter peak.

For the voxels that do not reach the pheromone saturation, the CAM gives an over-estimated value for the white matter percentage but it is important to remark that the voxels that are wrongly segmented with a normalized difference from the gold standard larger than 0.5 represent only the 3.5% of the brain volume.

Changes in the pheromone deposition rule were tested to make the CAM more general and more selective: in particular a Gaussian pheromone deposition rule was tried.

The mean and the standard deviation values are obtained from the histogram of the intensity of the image to be analyzed (fig. 10).

With this Gaussian configuration the CAM segmentation power increases. The comparison between the results obtained with the high intensity pheromone deposition rule and the Gaussian one is shown in fig. 11.

The ROC curve of the Gaussian configuration reaches very high values (*i.e.* $S = 0.989$) with a small contamination (*i.e.* $C = 0.03$) and the corresponding distribution of WM-GS
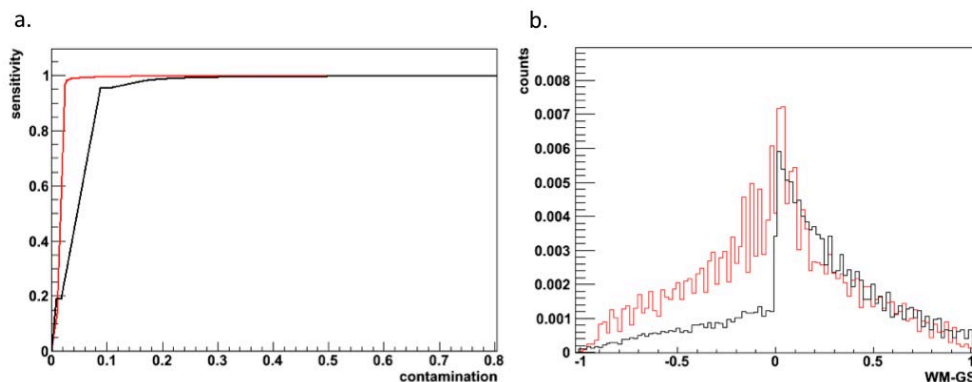

Fig. 11. – (Colour on-line) Comparison between the CAM result obtained with a pheromone deposition rule proportional to the image intensity (black line) and the CAM result given by a Gaussian one (red line): a. ROC curve for the voxels that reach the pheromone saturation (*i.e.* voxels segmented as 100% of white matter); b. difference between the CAM white-matter estimate (WM) and the gold standard value (GS) normalized to the 100% of white matter.

shows a peak centered at 0. As in the previous configuration, the voxels that are wrongly segmented with a normalized difference from the gold standard larger than 0.5 represent only few percent (*i.e.* 5%) of the voxels that belong to the brain.

5. – Conclusions

The CAM results obtained segmenting artificial objects and lung CTs show that the algorithm is able to reconstruct complex structures with unknown characteristics.

The first results on the MRI images for the white matter segmentation confirm the CAM adaptability to different kinds of images, regardless of their dynamic range.

Two different pheromone deposition rules were used: the first, taken from the artificial objects and the lung CTs applications, makes the CAM able to segment volume with a high intensity; the second, using a new Gaussian pheromone deposition rule, makes it possible to segment volumes with any values of average intensity (*e.g.* white matter, grey matter or cerebrospinal fluid).

With this second configuration, the CAM segmentation power for the voxels that are 100% white matter increases.

The CAM capability to determine the percentage of white matter in the voxels that do not reach the pheromone saturation was also analyzed. The results are encouraging but, for a satisfactory quantitative segmentation, improvements are required.

In the future, the method will be applied to real MRI images and the analysis of hippocampal volume, one of the most relevant brain structures for the assessment of the development of Alzheimer's disease.

REFERENCES

[1] CERELLO P., CHERAN S. C., BAGNASCO S., BELLOTTI R., BOLANOS L., CATANZARITI E., DE NUNZIO G., FANTACCI M. E., FIORINA E., GARGANO G., GEMME G., LÓPEZ TORRES E., MASALA G. L., PERONI C. and SANTORO M., *Pattern Recogn.*, **43** (2010) 1476.

[2] CHIALVO D. and MILLONAS M., *How swarms build cognitive maps*, in LUC STEELS (Ed.), *The Biology and Tecnology of Intelligent Autonomous Agents*, Vol. **144** (NATO ASI Series, 1995) pp. 439–450.

[3] RAMOS V. and ALMEIDA F., *Artificial ant colonies in digital image habitats a mass behaviour effect study on pattern recognition*, in *Proceedings of ANTS 2000, 2nd International Workshop on Ant Algorithms (From Ant Colonies to Artificial Ants), Belgium, 2000*, pp. 39–43.

[4] BOCCHI L., BALLERINI L. and HÄSSLER S., *A new evolutionary algorithm for image segmentation*, in *Lect. Notes Comput. Sci.*, Vol. **3449** (Springer, Berlin) 2005, pp. 264–273.

[5] SCHOONDERWOERD R., HOLLAND O. E., BRUTEN J. L. and ROTHKRANTZ L. J. M., *Adapt. Behav.*, **2** (1996) 169.

[6] DORIGO M., *Biosystems*, **43** (1997) 73.

[7] http://anode09.isi.uu.nl.

[8] PICOZZI G., PACI E., LOPEZ PEGNA A., BARTOLUCCI M., ROSELLI G., DE FRANCISCI A., GABRIELLI S., MASI A., VILLARI N. and MASCALCHI M., *Radiol. Med.*, **109** (2005) 17.

[9] http://imaging.cancer.gov/programsandresources/InformationSystems/LIDC.

[10] http://mouldy.bic.mni.mcgillca/brainweb/.